Article

Journal of
Nanoscience and Nanotechnology
Vol. 16, 12904–12909, 2016
www.aspbs.com/jnn

$Ni–CeO_2–ZrO_2$ Catalysts for Water Gas Shift Reaction: Effect of CeO_2 Contents and Reduction Temperature

Busaya Chamnankid[1], Karin Föttinger[2], Günther Rupprechter[2], and Paisan Kongkachuichay[1,3,*]

[1] Department of Chemical Engineering, Kasetsart University, Jatujak, Bangkok 10900, Thailand
[2] Institute of Materials Chemistry/Physical Chemistry Division, Vienna University of Technology, Getreidemarkt 9/1060 Vienna, Austria
[3] Center for Advanced Studies in Nanotechnology and Its Applications in Chemical, Food and Agricultural Industries, Kasetsart University, Bangkok 10900, Thailand

$Ni–CeO_2–ZrO_2$ catalysts with 5 wt% of Ni and different amounts of CeO_2 were prepared by an incipient wetness impregnation. The synthesized materials were tested for their activities for the water gas shift reaction (WGS) which was carried out at 200–400 °C with the reactants consisting of 3% CO and 7% H_2O. The effect of reduction temperatures (350, 400 and 500 °C) and amount of CeO_2 (0–20 wt%) on the CO_2 conversion were investigated. The prepared catalysts were characterized their physical and chemical properties via X-ray Diffraction, N_2 physisorption, H_2 chemisorption and *in situ* diffuse reflection infrared Fourier transform spectroscopy (DRIFTS). It was found that the reduction temperature and loaded CeO_2 content affected the surface area and dispersion of metal. Moreover, based on DRIFTS study, the formate species were found to be the important intermediates in the WGS reaction. The highest conversion of CO_2 at 71% was achieved when using $Ni–CeO_2–ZrO_2$ with 10% CeO_2 reduced at 400 °C.

Keywords: WGS, Nickel, Cerium Oxide, Zirconium Oxide, Catalysts.

1. INTRODUCTION

CeO_2-based catalyst is widely used as the support in many reactions, such as ethanol steam reforming,[1–7] steam reforming of CH_4,[8,9] three way catalysts,[10–13] hydrogen production,[14] and water gas shift (WGS) reaction.[11–13,15–18] Since CeO_2 can release/acquire oxygen through redox processes involving the Ce^{4+}/Ce^{3+} couple, it provides a way to increase the efficiency of CO oxidation for the water gas shift reaction (WGS). However, CeO_2 is fragile at high temperature, resulting in decreasing of surface area and also adsorption of reactants on the catalysts after severe aging. Therefore, the use of $CeO_2–ZrO_2$ mixed oxides are attracted by the researchers owing to their high thermal stability and reducibility, which provide higher catalytic performances.[19–21] Nevertheless, the support composition of $CeO_2–ZrO_2$ should be of concern due to the WGS reaction passing through a formate associative mechanism.[22,23] The reduction temperature is one of other factors that must be considered. Various pretreatment temperatures result in the dispersion of metal particles since a sintering effect might occur.[24] The higher percentage of metal dispersion leads to a higher metallic surface area which increases the chance of reactants to be adsorbed and reacted. For these reasons, in this work, the $CeO_2–ZrO_2$ based catalysts were tested for WGS reaction by using Ni as an active metal, and the effect of CeO_2/ZrO_2 contents and reduction temperatures on the catalytic activity were investigated.

*Author to whom correspondence should be addressed.

2. MATERIALS AND METHODS

2.1. Catalyst Preparation

All catalysts used in this work were synthesized from $Zr(OH)_4$ (MEL chemicals XZO 880/01), $Ce(NO_3)_3 \cdot 6H_2O$, and $Ni(NO_3)_2 \cdot 6H_2O$. Firstly, $Zr(OH)_4$ was calcined with a heating rate of 2 °C/min to 700 °C and kept at this temperature for 2 h. The suitable amount of $Ce(NO_3)_3 \cdot 6H_2O$ was dissolved in water in order to prepare 0–20 wt% of CeO_2 and then mixed with the ZrO_2-based support. After that the suspension was dried and calcined at 450 °C for 2 h. The obtained yellow powder was mixed with $Ni(NO_3)_2$ solution in order to obtain 5 wt% Ni in the final catalyst

1533-4880/2016/16/12904/006 doi:10.1166/jnn.2016.13798

powder which then was calcined at 450 °C for 2 h. This amount of Ni was adopted following our previous work.[25]

2.2. Catalyst Characterization

X-ray diffraction (XRD) patterns of all samples were obtained by using a PANalytical XPERT-PRO diffractometer with Cu Kα radiation operating at 40 kV and 40 mA, using 2θ scanning from 10 to 80° with a step of 0.02°.

In order to measure the specific surface area of nickel on ZrO_2 samples, hydrogen chemisorption was performed in the ASAP 2020 C Micromeritics. First, 0.6 g of fresh catalyst was reduced in hydrogen for half an hour at 400 °C and then it was evacuated at the same temperature for another 30 minutes and cooled down to 30 °C to perform a leak test. The analysis was performed at 30 °C at hydrogen pressures between 75 and 775 mbar and was repeated once in order to isolate the chemisorption isotherm. In order to study the effect of reduction temperature on the metallic properties, all samples were analyzed after pretreatment in various temperature range including 350, 400, and 500 °C.

BET surface area and porosity of the supports and catalysts were determined by nitrogen adsorption at −196 °C applying a Quantachrome Autosorb-1C instrument. The specific BET (SBET) was estimated for P/P_0 values between 0.05–0.30. The average pore diameter and the total pore volume were obtained from adsorption data at P/P_0 of 0.99.

In situ infrared spectroscopy of adsorbed carbon monoxide as a probe molecule was used to determine the oxidation state of Ni metal, the interaction between metal and support, and also all the chemical compounds produced during the reaction occurred. The spectra were obtained in the range of 4000 to 1000 cm^{-1} by averaging 128 scans with an aperture of 1.5 mm. Limitations of the equipment prevented operating at a temperature up to 400 °C as in the real reaction condition. However, the obtained data could be expected to perform in the same trend.

2.3. Catalytic Activity Test

The catalytic activities for water gas shift reaction were tested in a fixed bed reactor at atmospheric pressure and were carried out in the temperature region of 300–500 °C. Typically, 0.5 g of catalyst was placed between two quartz glass wool plugs inside the quartz tube which the temperature was controlled by thermocouple connected with Eurotherm temperature controller. The sample was reduced at two different temperatures of 400 and 500 °C with 5% H_2 in He for 1 h. After reduction process the reactant gases consisting of 3% CO, 7.5% H_2O balance with He were fed into the reactor at total flow rate of 60 ml/min. Gases products (CH_4, CO, and CO_2) were detected and analyzed with a HP 6890 Series GC system using HP-PLOT Q column and a flame ionization detector (FID). The amount of H_2 produced was measured by a Pfeiffer Prisma Plus (QMG 220 F1) mass spectrometer.

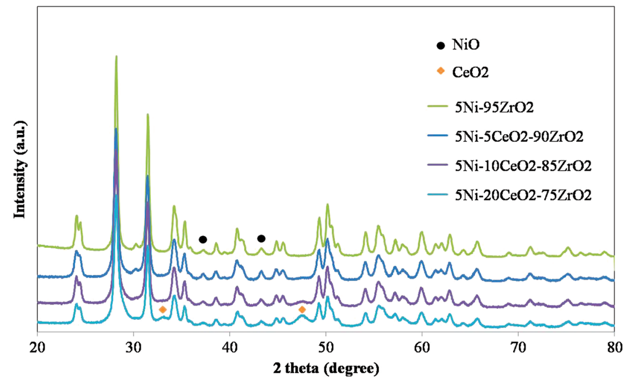

Figure 1. XRD patterns of Ni/CeO_2–ZrO_2 at various amount of CeO_2.

3. RESULTS AND DISCUSSION

3.1. Physical and Chemical Properties of Catalysts

Figure 1 shows the XRD spectra of all samples; it was found that all of them exhibited the same pattern which could be identified the existence of major component ZrO_2. Also there are small peaks demonstrated at $2\theta \approx$ 37.5 and 43.2° representing the occurrence of NiO,[26] while the peaks at around $2\theta \approx 33.4$ and 47.9° can be signified the presence of CeO_2 phase.[27] The intensity of CeO_2 peaks increased with the increasing amount of CeO_2, while NiO peaks were slightly decreased. This means the amount of CeO_2 brought about the formation of a smaller crystallite size of NiO, which could be accounted for the enhancing of metal dispersion.

The Ni surface area, crystallite size and metal dispersion of all samples obtained from H_2 chemisorption are shown in Table I. At the lowest reduction temperature 350 °C, it was found that the metallic surface and metal dispersion increased with the increasing of CeO_2, these results were

Table I. Properties of Ni-catalysts determined by H_2 chemisorption after reduction at 350, 400, and 500 °C.

	Metallic surface area m^2/(g of metal)	Metallic surface area m^2/(g of sample)	Crystallite size (nm)	Ni dispersion (%)
Reduction temp 350 sample				
5Ni–95ZrO_2	15.0493	0.7525	44.78638	2.2603
5Ni–5CeO_2–90ZrO_2	17.2204	0.861	39.13997	2.5864
5Ni–10CeO_2–85ZrO_2	26.3771	1.3189	25.55267	3.9617
5Ni–20CeO_2–75ZrO_2	42.5257	2.1263	15.84939	6.3871
Reduction temp 400 sample				
5Ni–95ZrO_2	31.4000	1.5700	22.89938	4.7367
5Ni–5CeO_2–90ZrO_2	40.9245	2.0462	16.46949	6.1466
5Ni–10CeO_2–85ZrO_2	46.5011	2.3251	14.49439	6.9842
5Ni–20CeO_2–75ZrO_2	24.5184	1.2259	27.48978	3.6825
Reduction temp 500 sample				
5Ni–95ZrO_2	9.5205	0.476	70.79494	1.4299
5Ni–5CeO_2–90ZrO_2	26.5929	1.3296	25.34531	3.9941
5Ni–10CeO_2–85ZrO_2	18.4282	0.9214	36.57475	2.7678
5Ni–20CeO_2–75ZrO_2	17.7335	0.8867	38.00749	2.6635

Table II. Properties of Ni-catalysts with various amount of CeO_2 measured by nitrogen sorption (use DR equation to calculate micropore volume and surface area).

Sample	S_{BET} (m^2/g)	BJH V_t (cc/g)	Avg. D (nm)
100ZrO_2	36.60	0.18	NA
5Ni–95Zr	37.21	0.51	17.34
5Ni–5Ce–90Zr	46.20	0.59	14.41
5Ni–10Ce–85Zr	53.55	0.33	12.17
5Ni–20Ce–75Zr	57.74	0.25	9.42
100CeO_2	104.4	0.34	12.15

correlated with the data obtained from XRD spectra as shown in Figure 1. As a lesser amount of CeO_2 was added, a larger Ni cluster was achieved, while the sample with the highest CeO_2 loaded, 5Ni–20CeO_2–75ZrO_2, possessed the largest surface area and the highest metal dispersion. Since CeO_2 held the cationic property after reduction process, the small Ni particles were anchored to the ZrO_2 surface.

When the process was performed at reduction temperature of 400 °C, all metal particles were completely reduced and H_2 molecules were adsorbed on the Ni surface. However, at higher temperature, the surface energy of Ni particles was also increased; accordingly, the smaller Ni particle presented, the higher surface area and reactivity were obtained. Based on this criterion, in order to reduce Gibbs free energy, the small Ni particles attempted to merge to each other creating the larger particles and decreasing the total surface area. As a result, 5Ni–20CeO_2–75ZrO_2, having the highest CeO_2 loaded and showing the smallest particle size when it was reduced at 350 °C, exhibited the largest particles and lowest Ni dispersion after it was reduced at 400 °C. In addition, at too high reduction temperature of 500 °C, not only the criterion mentioned above was considered but also the sintering effect was affected as well. In this way, the metallic surface area and Ni dispersion were decreased in all the samples as shown in Table I.

Table II shows the physical properties of all samples. It was found that the incorporation of CeO_2 to ZrO_2 caused a significance increase in surface area and a significance decrease in pore diameter and pore volume. The data revealed that the average pore diameter decreased with increasing amount of CeO_2, due to the deposition of CeO_2 on the surface of ZrO_2 support, which led to the decreasing of pore volume.

3.2. Catalytic Activity

CO_2 conversions of 5Ni–10CeO_2–85ZrO_2 reduced at various temperatures including 350, 400 and 500 °C are shown in Figure 2(a). Samples were tested the catalytic activities after reduced for 1 h in 5% H_2 balance with He. Clearly, when the reaction was operated at starting temperature of 400 °C, all samples exhibited the highest CO_2 conversions and then started to be decreased as the temperature was decreased to 200 °C. However, 5Ni–10CeO_2–85ZrO_2 reduced at 400 °C showed the highest CO_2 conversion at about 71% while the corresponding conversion of CO_2 was only 23 and 31% over the samples reduced at 500 and 350 °C, respectively. These results accounted for the sintering effect of support during the reduction process at severe condition (500 °C) and uncompleted reduction at too low temperature (350 °C). Data also related to the metallic chemical properties, which were explained and discussed earlier.

When the CeO_2 contents were taken into account, the samples prepared with different amounts of CeO_2 were reduced at 400 °C and were carried out in the temperature range of 200–400 °C; the catalytic activities are shown in Figure 2(b). From the data, it was found that the addition of CeO_2 has a significant influence on the CO_2 conversion by increasing CO_2 conversion at any temperature. However, the conversion was increased only if the amount of CeO_2 was increased from 0–10 wt%. Samples showed a high metal dispersion and large metallic surface area, providing the chances of reactant gases to be adsorbed on the active metal and dissociate to form gas products. Conversely, when the CeO_2 was added up to 20 wt%, the catalytic activity was dropped. This effect can be explained according to a low metal dispersion and metallic surface area, causing from the sintering effect, as previously shown in Table II. In addition, it was clearly seen that at low temperature (below 250 °C), the amount of CeO_2 did not take

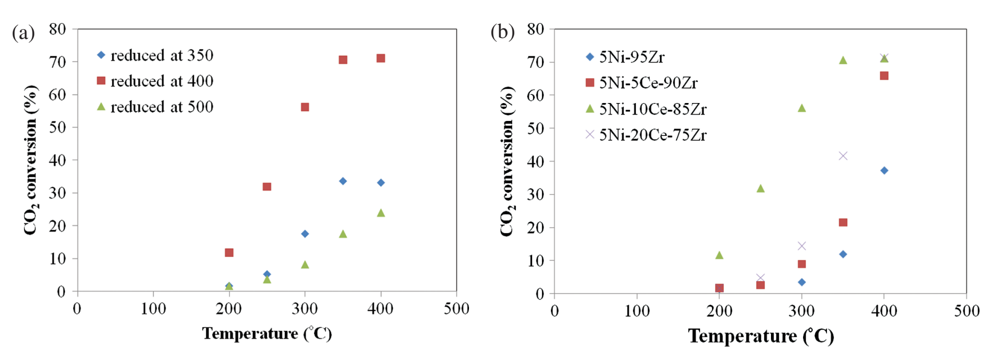

Figure 2. CO_2 conversions obtained by using (a) 5Ni–10CeO_2–85ZrO_2 reduced at various temperatures (b) catalysts which contained different amount of CeO_2 and ZrO_2 reduced at 400 °C.

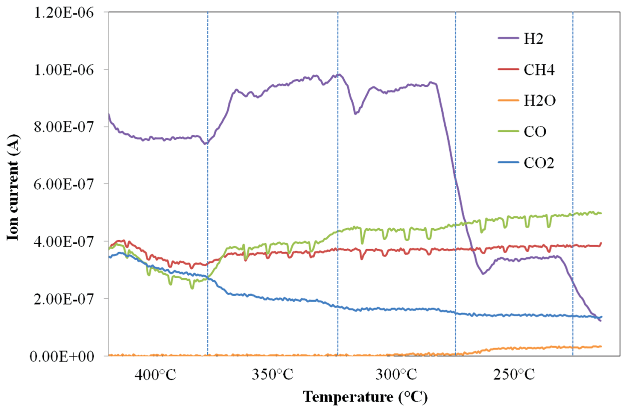

Figure 3. Mass spectroscopy of 5Ni–10CeO_2–85ZrO_2 reduced at 400 °C and operated at different reaction temperature.

much effect on the catalytic activity. Based on the CO_2 conversion (Fig. 2(b)), the 5Ni–10CeO_2–85ZrO_2 catalyst was chosen for further analysis due to its highest performance.

In this work, the production of H_2 could not be determined by using a GC; therefore, a mass spectroscopy (MS) was chosen to detect the qualitative value of H_2 formation instead. The MS of 5Ni–10CeO_2–85ZrO_2 after reducing at 400 °C and operating in the reaction temperature range of 200–400 °C are shown in Figure 3. From the obtained spectra, it was clearly seen that there was a high conversion of CO and H_2O to the gas products H_2 and CO_2 at relative high temperature. The conversion of CO was slightly decreased as the temperature decreased and the activity of the catalysts was dropped immediately when a temperature of 250 °C was reached. Moreover, CH_4 was produced as a side product during carrying out the WGS reaction. CH_4 was formed from the hydrogenation process of CO/CO_2 in a methanation reaction as shown in following reactions:[28]

$$CO + 3H_2 \leftrightarrow CH_4 + H_2O$$

$$CO_2 + 4H_2 \leftrightarrow CH_4 + 2H_2O$$

$$2CO + 2H_2 \leftrightarrow CH_4 + CO_2$$

There are reports published that the WGS reaction occurs via a formate associative mechanism, having a surface formate decomposition as a rate limiting step. At low temperature, the stability of formate species on support surface was increased, resulting in the remaining of formate species on metal surface and causing a low catalytic activity.[22,23,29] The formate associative mechanism will be discussed in Section 3.3.

3.3. *In Situ* DRIFTS

Figure 4 shows *in situ* DRIFTS of CO adsorption on 5Ni–10CeO_2–85ZrO_2 catalyst, which were recorded after the sample was reduced by heating up at a rate of 10 °C/min to 350 °C in the 5% H_2 in He. The sample was kept at this temperature for 60 min before cooling down to 30 °C. Then CO gas was introduced into the sample's cell for 15 min in order to detect CO adsorption on Ni before it was purged with He. Subsequently, the sample was reduced again at 350 °C before the reaction was performed in the temperature range of 50–300 °C. When the sample was first reduced, the spectra exhibited the characteristic peak representing CO adsorption on Lewis acid sites of oxidized ZrO_2-based at 2186 cm^{-1} while the peak in the region of 2170–2180 cm^{-1} could be assigned to adsorption band of weak Ni(II)–CO complex.[30] The two bands detected at 2067 and 1963 cm^{-1} correspond to the CO adsorbed on metallic Ni, the former pointing out the adsorbed CO in linear form and the latter showing bridge-bonded CO.[30,31] In addition, there was a band at about 1634 cm^{-1} representing bicarbonate formate species. After He was purged, all peaks still existed, which could be explained by the fact that CO was strongly adsorbed on the support.

During the WGS reaction, DRIFTS spectra were detected as the temperature decreased. Clearly, there were peaks presented in the region of 1300–1650 cm^{-1} indicating the formation of bicarbonate and mono-bidentate formate species such as HCO_3, CH_3CHO, and CH_3COCH_3. It was found that the peaks of monodentate formate

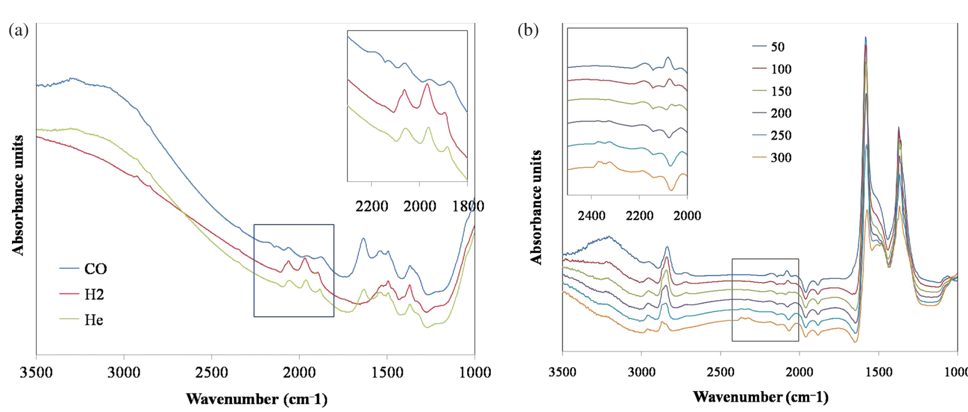

Figure 4. (a) CO adsorption on 5Ni–10CeO_2–85ZrO_2 after reduction at 350 °C and operated at 30 °C, and (b) *In situ* DRIFTS of CO adsorption on 5Ni–10CeO_2–85ZrO_2 after reduction at 350 °C and tested for the WGS reaction at 30–300 °C.

appeared at 1,572 and 1481 cm^{-1} while the bidentate formate species were observed at 1512 and 1367 cm^{-1}. The presence of these species was confirmed by the peaks exhibited in the region of 2800–3000 cm^{-1} associated to C–H stretching vibration of adsorbed formate species. Besides, the intensity of all that peaks increased with the decreasing of temperature. There were two bands presented at about 2322 and 2369 cm^{-1} indicating the existence of asymmetric stretching of CO_2 and the peaks intensities decreased with the falling of temperature which totally disappeared at 150 °C. These results could be explained as follows: As the reaction occurred, the bicarbonate formate species were decomposed into bidentate formate species which finally were broken down to produce H_2 and CO_2. Therefore, the bands of formate species decreased and the bands related to CO_2 increased remarkably, and it was probable to be concluded that the formate species acted as the intermediates for WGS reaction. Some researchers studied and proposed that the formate decomposition rate was considered to be the rate limiting step; as a result, with a faster formate decomposition there is a greater amount of CO_2 produced.[29,32] However, the rate formation of formate species which was the initial step for WGS reaction would increase with the concentration of surface OH groups which were enhanced to be formed on ceria sites. Therefore, the catalytic activity was increased as the higher amount of CeO_2 was loaded until 20% of CeO_2 was reached, as shown in Figure 2.

Another factor that should be considered was the stability of formate species on the support; the carbonate species with COO vibrations increased their stabilities with the ZrO_2 contents. They were strongly and irreversibly adsorbed on the support at low temperature and more easily to be decomposed toward CO_2 as the temperature increased. Obtained data were confirmed by the MS spectra (Fig. 3), which presented that the CO_2 formation was favored at high temperature and was decreased as the temperature decreased. These results agree with the work of Lin et al.,[28] who reported that using Ni catalyst at low temperature (<250 °C), CH_4 preferred to be formed rather than CO_2.

4. CONCLUSIONS

The addition of CeO_2 to ZrO_2 not only enhanced the Ni dispersion and Ni surface area but also created a greater number of ceria sites during the reduction process. These sites were considered to be active areas that promote the formation of OH groups which then react with adsorbed CO to create the intermediate formate species for WGS reaction. Beside the adding CeO_2, the reduction temperature was an important factor for the catalytic performance as well. At a too high reduction temperature of 500 °C, the sintering effect showed a greater impact than that of added CeO_2 while at too low reduction temperature of 350 °C the Ni metal was not completely reduced, resulting in the decreasing of catalytic activity. It was found that $5Ni–10CeO_2–85ZrO_2$, which is the sample containing 10 wt% of CeO_2, showed the highest CO_2 conversion of 71% after it was reduced at 400 °C.

Acknowledgments: This work was financially supported by the Thailand Research Fund through the Royal Golden Jubilee Ph.D. Program (Grant No. PHD/0182/2551) for Busaya Chamnankid.

References and Notes

1. W. Cai, F. Wang, C. Daniel, A. C. van Veen, Y. Schuurman, C. Descorme, H. Provendier, W. Shen, and C. Mirodatos, *J. Catal.* 286, 137 (**2012**).
2. N. Rao Peela, A. Mubayi, and D. Kunzru, *Chem. Eng. J.* 167, 578 (**2011**).
3. F. Wang, W. Cai, H. Provendier, Y. Schuurman, C. Descorme, C. Mirodatos, and W. Shen, *Inter. J. Hydrogen Energy* 36, 13566 (**2011**).
4. Q. Liu, Z. Liu, X. Zhou, C. Li, and J. Ding, *J. Rare Earth* 29, 872 (**2011**).
5. F. Wang, W. Cai, Tana, H. Provendier, Y. Schuurman, C. Descorme, C. Mirodatos, and W. Shen, *Appl. Catal. B-Environ.* 125, 546 (**2012**).
6. J.-Y. Siang, C.-C. Lee, C.-H. Wang, W.-T. Wang, C.-Y. Deng, C.-T. Yeh, and C.-B. Wang, *Inter. J. Hydrogen Energy* 35, 3456 (**2010**).
7. P. Ciambelli, V. Palma, and A. Ruggiero, *Appl. Catal. B-Environ.* 96, 190 (**2010**).
8. H.-W. Kim, K.-M. Kang, H.-Y. Kwak, and J. H. Kim, *Chem. Eng. J.* 168, 775 (**2011**).
9. W.-S. Dong, H.-S. Roh, K.-W. Jun, S.-E. Park, and Y.-S. Oh, *Appl. Catal. A-Gen.* 226, 63 (**2002**).
10. Z. Zhan, X. Liu, H. He, L. Song, J. Li, and D. Ma, *J. Rare Earth.* 31, 750 (**2013**).
11. R. Ran, H. Zhang, X. Wu, J. Fan, and D. Weng, *J. Rare Earth.* 32, 108 (**2014**).
12. B. Shen, X. Zhang, H. Ma, Y. Yao, and T. Liu, *J. Environ. Sci.* 25, 791 (**2013**).
13. S. O. Soloviev, P. I. Kyriienko, and N. O. Popovych, *J. Environ. Sci.* 24, 1327 (**2012**).
14. S. Lorentzou, G. Kastrinaki, C. Pagkoura, and A. G. Konstandopoulos, *Nanosci. Nanotechnol. Lett.* 3, 697 (**2011**).
15. K. Chayakul, T. Srithanratana, and S. Hengrasmee, *J. Mol. Catal. A-Chem.* 340, 39 (**2011**).
16. V. M. Shinde and G. Madras, *Appl. Catal. B-Environ.* 123–124, 367 (**2012**).
17. V. M. Shinde and G. Madras, *Appl. Catal. B-Environ.* 132–133, 28 (**2013**).
18. R. Si, J. Raitano, N. Yi, L. Zhang, S.-W. Chan, and M. Flytzani-Stephanopoulos, *Catal. Today* 180, 68 (**2012**).
19. F. Vindigni, M. Manzoli, T. Tabakova, V. Idakiev, F. Boccuzzi, and A. Chiorino, *Appl. Catal. B-Environ.* 125, 507 (**2012**).
20. H. Li, Y. Bi, J. Yan, L. Zhang, and X. Yin, *Catal. Commun.* 42, 45 (**2013**).
21. R. Pilasombat, H. Daly, A. Goguet, J. P. Breen, R. Burch, C. Hardacre, and D. Thompsett, *Catal. Today* 180, 131 (**2012**).
22. C. M. Kalamaras, S. Americanou, and A. M. Efstathiou, *J. Catal.* 279, 287 (**2011**).
23. K. C. Petallidou, C. M. Kalamaras, and A. M. Efstathiou, *Catal. Today* 228, 183 (**2014**).
24. S. Velu and S. Gangwal, *Solid State Ionics* 177, 803 (**2006**).

25. B. Chamnankid, K. Föttinger, G. Rupprechter, and P. Kongkachuichay, *Chem. Eng. Technol.* 37, 2139 **(2014)**.
26. Y. Li, Q. Fu, and M. Flytzani-Stephanopoulos, *Appl. Catal. B-Environ.* 27, 179 **(2000)**.
27. K. Chayakul, T. Srithanratana, and S. Hengrasmee, *Catal. Today* 175, 420 **(2011)**.
28. J. H. Lin, P. Biswas, V. V. Guliants, and S. Misture, *Appl. Catal. A-Gen.* 387, 87 **(2010)**.
29. C. I. Vignatti, M. S. Avila, C. R. Apesteguía, and T. F. Garetto, *Catal. Today* 171, 297 **(2011)**.
30. M. Mihaylov, K. Chakarova, and K. Hadjiivanov, *J. Catal.* 228, 273 **(2004)**.
31. A. V. Ivanov and L. M. Kustov, *Russian Chem. Bull.* 47, 394 **(1998)**.
32. J. Li, J. Chen, W. Song, J. Liu, and W. Shen, *Appl. Catal. A-Gen.* 334, 321 **(2008)**.

Received: 8 October 2014. Accepted: 5 May 2015.